



## Dynamic impact of boulders on different types of concrete dam

Zhu-jun FENG, Xiu-li WANG, Yong-hong RAN

View online: <https://doi.org/10.1007/s11629-022-7419-1>

---

### Articles you may be interested in

[Characteristics of debris flow impact on a double-row slit dam](#)

Journal of Mountain Science. 2023, 20(2): 415 <https://doi.org/10.1007/s11629-022-7462-y>

[Rapid prediction models for 3D geometry of landslide dam considering the damming process](#)

Journal of Mountain Science. 2023, 20(4): 928 <https://doi.org/10.1007/s11629-022-7906-z>

[Refined mathematical model for the breaching of concrete-face sand-gravel dams due to overtopping failure](#)

Journal of Mountain Science. 2023, 20(3): 670 <https://doi.org/10.1007/s11629-022-7490-7>

[Depth-resolved numerical model of dam break mud flows with Herschel-Bulkley rheology](#)


Journal of Mountain Science. 2022, 19(4): 1001 <https://doi.org/10.1007/s11629-021-7218-0>



[Dynamic response analysis of blocks-combined dam under impact load](#)


Journal of Mountain Science. 2020, 17(11): 2827 <https://doi.org/10.1007/s11629-019-5619-0>

Original Article

## Dynamic impact of boulders on different types of concrete dam

**FENG Zhu-jun**<sup>1</sup>  <https://orcid.org/0000-0003-2174-3770>; e-mail: zhujunfeng@lut.edu.cn

**WANG Xiu-li**<sup>1,2\*</sup>  <https://orcid.org/0000-0002-7548-6733>;  e-mail: wangxl@lut.edu.cn

**RAN Yong-hong**<sup>1,2</sup>  <https://orcid.org/0000-0003-4642-3132>; e-mail: ransongayst@126.com

\*Corresponding author

<sup>1</sup> School of Civil Engineering, Lanzhou University of Technology, Lanzhou 730050, China

<sup>2</sup> Western Center of Disaster Mitigation in Civil Engineering of Ministry of Education, Lanzhou University of Technology, Lanzhou 730050, China

**Citation:** Feng ZJ, Wang XL, Ran YH (2022) Dynamic impact of boulders on different types of concrete dam, Journal of Mountain Science 19(10). <https://doi.org/10.1007/s11629-022-7419-1>

© Science Press, Institute of Mountain Hazards and Environment, CAS and Springer-Verlag GmbH Germany, part of Springer Nature 2022

**Abstract:** Concrete dams are reliable when subjected to static loads such as earth pressure and water pressure. However, the dam failure would be abrupt and catastrophic if it is impacted by boulders. This study simulated the dynamic response of flat dam, concave dam, and convex dam under the impact of boulders by using ANSYS/LS-DYNA finite element software. In the numerical simulation, the strain rate effect under the impact load is considered, and Holmquist-Johnson-Cook (HJC) model—a dynamic damage constitutive model is applied to concrete materials. Results show that the peak impact force of concave dam is minimum. Meanwhile, for different dam types (flat dam, concave dam, and convex dam) and impactor velocities (5, 10, and 15 m/s), the impact force fluctuates with the height of the impact point and it reaches the maximum value when the height of the impact point is 2/3 of the dam height. Numerical simulation mainly considers different masses and velocities and obtains empirical formulae of impact force for three dam types. The established empirical formula for the flat dam is compared with the existing classical formula and several similar experimental tests. It was found that the newly empirical formulae are reasonable and effective, and it provides design suggestions for similar concrete dams.

**Keywords:** Concrete dam; Boulders impact; Impact force; Numerical simulation; HJC constitutive model

### 1 Introduction

In recent years, irrational human economic activities have disrupted the ecological balance and caused environmental degradation, which has caused disasters such as mountain collapses, landslides, and mudslides. These disasters often wash away fields and damage houses, roads, bridges, and other building structures that people rely on for survival. They also cause heavy losses to the national economy, people's lives and property (Gang et al. 2019). Therefore, the analysis and prevention of geological hazards have been the focus of attention all over the world for many years (Ouyang et al. 2017; Gao et al. 2018; Wei et al. 2018; Wang et al. 2020a; Wang et al. 2020b; Su et al. 2022). From 1950 to 2021, geological hazards caused huge property losses and casualties all over the world, especially rockfall disasters (Dowling and Santi 2014; Ferrari et al. 2016; Gao et al. 2020; Cappadonia et al. 2021). Ulamiş et al. (2020) conducted a comprehensive mapping of slopes and provided mitigation methods by assessing rockfall hazards in the Ankara area. These include removing blocks from

**Received:** 17-Apr-2022

**1<sup>st</sup> Revision:** 16-May-2022

**2<sup>nd</sup> Revision:** 27-Jun-2022

**Accepted:** 25-Jul-2022

slopes, covering slopes with anchoring wire mesh, and building earthen walls to prevent possible rockfall damage to residents. Through a hazard assessment of rockfalls in mountainous urban areas of western Saudi Arabia, Othman et al. (2021) recommended protective measures to prevent and mitigate the impact of rockfall activities on similar areas. To reveal the collision and fragmentation mechanism in the evolution of high-speed fragments, Gang et al. (2019) proposed a two-dimensional block-terrain collision model in which a strong brittle rock block collides with a rigid plane. Kang et al. (2021) studied the kinematic characteristics of a rock avalanche in Wenchuan earthquake in 2008 and the rock collapse in Wen-jia valley and concluded that the main cause of the geological hazards is the collapse of check dams. Fig. 1 shows the damage to the dam after being impacted by boulders.

To mitigate geological disasters, different types of prevention and control structures have been designed, including gravity dams, rigid grid dams, and flexible cable net structures (Im et al. 2017; Huang and Zhang 2020; Gao and Tian 2020; Jin et al. 2021). Since the traditional gravity dam is easy to be damaged by boulders, it has a serious influence on the ecological environment. Therefore, scholars have done a lot of research on dam prevention and control. Shieh et al. (2008) proposed a new type of curved dam, which can enhance the impact resistance of the dam and effectively decrease the amount of concrete. Kim et al. (2017) proposed a closed dam with flaps and compared the dynamic characteristics with conventional dams, and the results show that the flapped baffle dam has the advantage of intercepting debris flow boulders. Gao et al. (2020) proposed a pre-stressed steel strand composite dam to effectively

resist the impact damage of boulders to it. Pla et al. (2020) compared the dynamic characteristics of a traditional reinforced concrete (RC) frame structure with a novel RC frame structure encased with shaped steel (NRCFS) through a series of impact load tests. The results show that the NRCFS has excellent impact resistance.

Moreover, the crucial factor to be considered in the design of the dam is the impact force. Therefore, the accurate determination and calculation of the impact force are significant. Particularly, the calculation of impact force is closely related to the development of contact theory and contact dynamics. In the late nineteenth century, Hertz (1881) proposed Hertz's theory of elasticity, which was limited to frictionless surfaces and perfectly elastic solids. On this basis, Yang et al. (1969) studied the application of Hertz contact law in plate impact problems, and contact forces of different materials are analyzed, based on this, it is proposed that viscoelastic plastic materials can be used as effective shock absorbers. Johnson (1985) published a book on contact mechanics suitable for engineering applications, which discussed in detail the calculation method of contact force between two objects. Yu et al. (2018) established the maximum impact force under rockfall impact through physical tests on different impact kinetic energies and elastic modulus of the rock and object. Liu et al. (2021) quantitatively identified the influence of block impact angle and shape on the impact effect of reinforced concrete (RC) shed. To understand the influence of the weight, size, shape, stiffness, material, and motion type of a collision object on the impact force mobilization characteristics, Nakajima et al. (2021) carried out a series of experiments. Luo et al. (2022) proposed a surface-to-

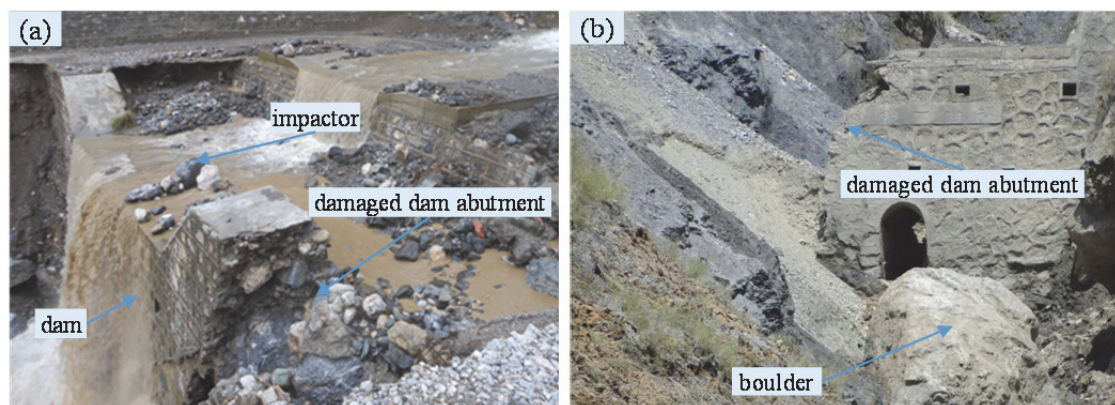


**Fig. 1** Damaged structures due to geological hazards in China: (a) Gravity dam at Shimian County, Ya'an City, Sichuan Province, China; (b) Gravity dam at Zhouqu County, Gannan Prefecture, Gansu Province, China. (Source from Yu (2016))

surface calculation method to estimate the maximum impact force, which takes into account the impact velocity, density, and size of boulders as well as the constitutive relationship of rock. In general, the dynamic response of different protective dams subjected to boulders and the contact force between them are considered in the above research, but the impact force under different dam types is rarely considered.

Although many researchers have explored the calculation method of impact force, the existing impact force calculation is only for the results of a flat dam under the impact (Nakajima et al. 2021; Luo et al. 2022). As known, geological disasters are complex, and dams with different structures and shapes need to be built under different geological environments. Additionally, the majority of dams are damaged due to large impact forces. Therefore, it is of great significance to study the impact force of different dam types against boulder impact for dam design, such as flat dams and arch dams. Despite the curved dams in common projects are loaded by the convex surface, the general design is subjected to the effect of uniform water pressure. When a curved dam is designed to be concave and subjected to local impact loads, the storage capacity of the retaining dam can be effectively increased, especially when it is subjected to multiple impact boulders. Therefore, it has certain research significance to study the impact load of different shapes under different circumstances.

In this paper, we consider the different impact directions of arch dams and analyze the dynamic response of the flat dam, concave dam, and convex dam under the impact of boulders. Based on the Holmquist-Johnson-Cook (HJC) dynamic damage model of concrete, the numerical simulation is carried out by using the ANSYS/LS-DYNA to study the impact force and damage mode of three different types of dams. In addition, for different dam types, impactor velocities, and diameters, we analyze the impact force when a boulder impacts the different heights of a dam. Finally, the empirical formulae of impact force of different dam types are put forward to provide suggestions for engineering design.

## 2 Materials and Methods

The nonlinear explicit dynamic analysis method was used to establish the finite element model (FEM)

by ANSYS/LS-DYNA, and the dynamic response of concrete dams under the impact of boulders was studied.

### 2.1 Modeling and meshing

According to the analysis results of Bozdağ (2022), it is determined that the maximum bouncing height of the rolling stone reaches 6.80 m. In addition, the width of the dam depends on the specific geological environment. This paper considers the geological environment of the small valley, the width and height of the model are determined as follows. The geometry of the flat dam is shown in Fig. 2(a). The width and height of the dam are 14 m and 7.5 m, respectively. Considering the storage requirements of blocking rocks and debris flow, the slope ratio of upstream surface is generally larger than that of downstream surface. In this paper, the dam size is designed according to the actual engineering of the debris flow disaster control project of Sanyanyu gully in Zhouqu County, Gansu Province, China. In this project, the upstream slope ratio is 1:0.35, and the downstream slope ratio range is between 1:0.1 and 1:0.2. Moreover, the Chinese standard T/CAGHP 021 (2018) also stipulates that the upstream face-slope ratio of the retaining dam is 1:0.4~1:0.8, and the downstream face-slope ratio is 1:0.05~1:0.2. Therefore, in the text, the upstream and downstream face slope of dams is 1:0.27 and 1:0.13, respectively.

In addition to a flat dam, due to the different geological environments, arch dams are considered. The plane dimension of the concave dam and convex dam are shown in Fig. 2(b). The inner arch radius of the arch dam is 8600 mm, and its central angle is 100 degrees. Particularly, the section size of the arch dam is the same as that of the flat dam, and its height is still 7.5 m. There are three reasons why we choose the same section of an arch dam and a flat dam. Firstly, the arch dam is designed based on the debris flow retaining dam, not for the large arch dam in water conservancy and hydropower engineering. The slope of the arch dam is relatively steep, and the main consideration is the application scope of the dam, which is suitable for rock disasters in small valleys. Secondly, debris flow dam height generally does not exceed 20 m, and the section form of an arch dam can also refer to a flat dam. Finally, it is better to design the same section to compare the dynamic response of three different dam types.



Due to the complex geometry of rock and mechanical behavior of dam under impact loading, it is necessary to select the appropriate element type when establishing the finite element model. The integrated reduced eight-node brick element is used for rock and dam. To simplify the simulation calculation, the following assumptions are made for the impactor: (1) the impactor is assumed to be a sphere; (2) the impactor is elastic and any damage is ignored; (3) the heat loss during impact is not considered.

Considering the stress distribution and impact energy of arch structures, this paper analyzes the impact of arch dams in two directions and compared the response of impact load. In the numerical simulation, the grid convergence research is to ensure the stability and accuracy of the solution. Therefore, it

is necessary to adjust the optimal mesh size to obtain accurate finite element results in the optimal calculation time. The convergence study includes the analysis of peak impact force and conservation of energy. The simulation results show that the hourglass energy of the model is the smallest when the grid size near the impact point is 50 mm. To ensure the calculation accuracy and efficiency at the same time, the grid transition was performed when the element has meshed. The grid size near the impact point was 50 mm, and the grid size far away from the impact point was 300 mm. The number of elements of the flat dam, concave dam, convex dam, and impact sphere was 240000, 200000, 240000, and 6912, respectively. The hexahedral mesh was divided by the mapping mesh method. The numerical models of three different types of dams are shown in Fig. 3.

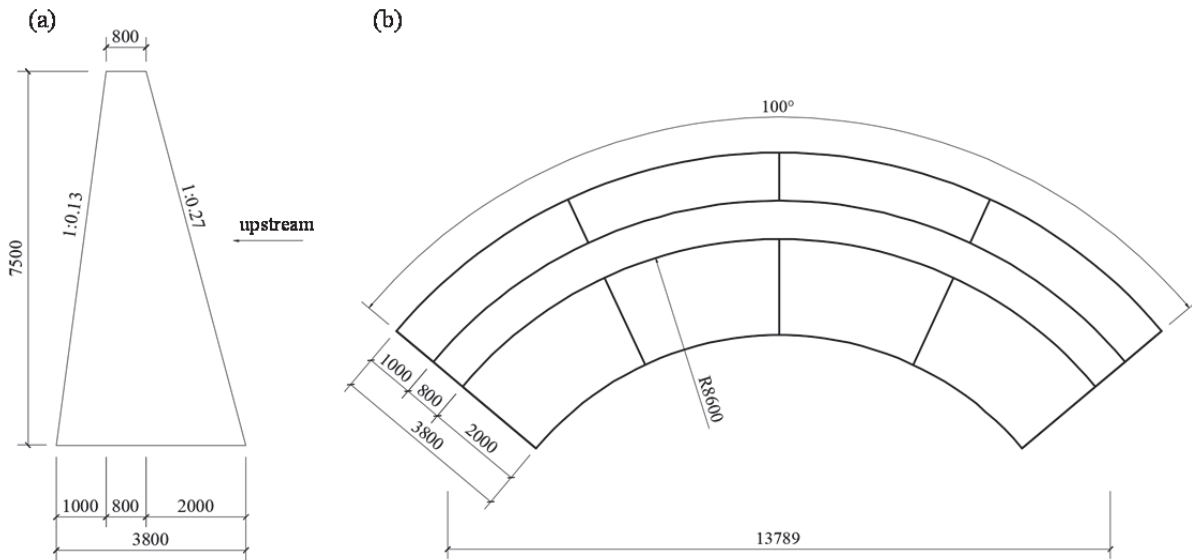


**Fig. 2** Dam geometry (unit: mm): (a) cross-section of the flat dam; (b) plane size of the concave dam and convex dam (the cross-section is the same as the flat dam).

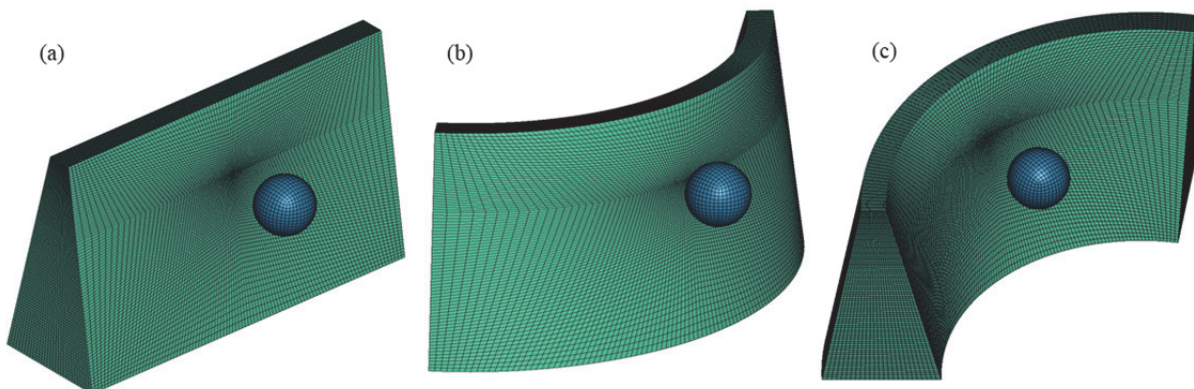


**Fig. 3** Numerical simulation model: (a) flat dam; (b) convex dam; (c) concave dam.

Fixed constraints were set at the bottom and on both sides of concrete dams, and the influence of the foundation was not considered. An erosion surface-to-surface contact (ESTS) was provided between the impact sphere and the concrete dam. The static friction coefficient between concrete and rock was 0.6, and the dynamic friction coefficient was 0.58 (Sekhar 2018). Since the impact force-time history curve is a short-time peak pulse, the calculation time step must be small. To better observe the dynamic response of the dam under impact loads, especially the damage form of the dam, after numerous trial calculations and observations, the solution time was set to 0.3 s, and the number of time steps was 1000. To ensure the correctness of the simulation, the energy of the whole system needs to be conserved. Due to the use of a reduced integral element in the explicit analysis of numerical simulation, the number of integral points is less than the actual number. When the calculation speed is accelerated, it will cause a zero-energy mode of the element, which results in hourglass energy and unreal oscillation of numerical simulation, so it is necessary to control the hourglass energy. Among them, when the hourglass energy is less than 5% of the internal energy, analysis results are valid and reliable. As such, to meet the hourglass performance requirements, hourglass control is carried out. The IHQ (i.e., hourglass control type) was set as 4 and the QM (i.e., hourglass coefficient) was 0.03.

## 2.2 Determination of impact mass and velocity

When analyzing the impact force, the key parameters include the difference between the impact mass and velocity, so this paper considers the impact of the different impact masses and velocities on the impact force. Referring to the actual engineering, the mass and velocity of the impactor selected in the simulation are determined.

Evans and Hungr (1993) found that the average diameter of boulders is 1.8 m by investigating the rockfall in Similkameen valley of British Columbia. Furthermore, according to the rockfall risk assessment of Kilistra settlement (Konya) in Turkey, the average diameter of rockfall is 3 m and the velocity of rockfall ranged from 1 m/s to 20 m/s (Bozdağ 2022). To sum up, when analyzing the impact force in this paper, the diameter range of the impactor is 1~3 m, and the velocity of the impactor ranges from 5 m/s to 15 m/s.

## 2.3 Material parameters and constitutive model

Numerical simulations were carried out by using software ANSYS/LS-DYNA to study the dynamic response of dams. The element type of the boulder was Solid164, which adopted an elastic model. The density, Young's modulus, and Poisson's ratio of the rock were 2500 kg/m<sup>3</sup>, 50 GPa, and 0.28, respectively. Because concrete dams are often built in places with harsh geological and construction environments, and the concrete strength grade has little effect on the impact resistance of structures, considering the actual construction factors, the concrete grade of dams is usually designed to be C25 (i.e., compressive strength grade of concrete is 25 MPa). The influence of damping on the impact force is not considered in the numerical simulation owing to the impact process being short.

The mechanical behavior of materials under dynamic loading is significantly different from the static load, and the strain rate effect needs to be considered. In addition, the research shows that the damage model is recommended when studying the failure process and mechanism of concrete gravity dams (Yan et al. 2021). The dynamic damage constitutive models of concrete commonly include the Taylor-Chen-Kuszmaul (TCK) model (Taylor et al. 1986), Holmquist-Johnson-Cook (HJC) model (Holmquist et al. 1993), Karagozian and Case (K&C) model (Malvar et al. 1997), Riedel-Hiermaier-Thoma (RHT) model (Riedel et al. 1999), and Continuous-Surface-Cap (CSCM) model (Murray 2007). The research results show that the HJC model can well simulate the dynamic response after the impact of drop weight (Long et al. 2018). Therefore, in this paper, the HJC constitutive model was used to simulate the impact response of concrete. This model uses an exponential function form of the yield surface and a three-stage state equation. It is considered that the compression damage consists of two parts: the plastic volumetric strain and the equivalent plastic strain. A strain rate amplification factor is added to the yield surface function to account for the expansion of the yield surface due to the increase in strain rate. High pressure, strain rate, and damage are considered in this model. The effects of plastic volumetric strain, equivalent plastic strain, and pressure are calculated. The pressure is calculated by volumetric strain and the compaction of the material is considered. Because this model can accurately describe the impact

mechanical behavior of concrete, it has been widely used in numerical simulation (Long et al. 2018; Wan et al. 2021). The equivalent strength expression for this model is shown in Eq. (1):

$$\sigma^* = [A(1-D) + BP^{*N}] [1 + C \ln \dot{\epsilon}^*] \quad (1)$$

where:  $\sigma^*$  is the normalized equivalent stress,  $\sigma^* = \sigma / f'_c$  and  $\sigma^* \leq S_{f_{max}}$ ,  $\sigma$  is the actual equivalent stress,  $f'_c$  is the uniaxial compressive strength of the material,  $S_{f_{max}}$  is the normalized maximum strength that can be achieved;  $A$ ,  $B$ ,  $C$ , and  $N$  are material constants,  $A$  is the normalized cohesive strength,  $B$  is the normalized pressure hardening coefficient,  $C$  is the strain rate coefficient,  $N$  is the pressure hardening exponent;  $D$  is the damage constant ( $0 \leq D \leq 1$ ), where 0 for no damage and 1 for broken;  $P^*$  is the normalized hydrostatic pressure,  $P^* = P / f'_c$ , where  $P$  is the actual hydrostatic pressure;  $\dot{\epsilon}^*$  is the dimensionless strain rate,  $\dot{\epsilon}^* = \dot{\epsilon} / \dot{\epsilon}_0$ , where  $\dot{\epsilon}$  is the actual strain rate, and  $\dot{\epsilon}_0$  is the reference strain rate, setting  $\dot{\epsilon}_0 = 1 \text{ s}^{-1}$ .

The \*MAT\_111 (\*MAT\_JOHNSON\_HOLMQUIST\_CONCRETE) in LS-DYNA denotes the HJC constitutive model. Among them,  $\rho_0$  is the material density, the shear modulus  $G$  is calculated according to  $G = E / (2(1 + \nu))$ , the bulk modulus is obtained from the formula  $K = E / (3(1 - 2\nu))$ ,  $T$  is the maximum tensile hydrostatic pressure,  $E_{fmin}$  is the amount of plastic strain before fracture,  $F_s$  is the failure type,  $P_c$  is the crushing pressure, where  $P_c = f'_c / 3$ ,  $\mu_c$  is the crushing volumetric strain, where  $\mu_c = P_c / K$  (Holmquist et al. 1993). Because value  $a = P_l / P_c \approx 50$ , then you can find the  $P_l$  value, where  $P_l$  is the locking pressure,  $\mu_l$  is the locking volumetric strain. Referring to relevant manuals and literature, 21 parameters of the HJC dynamic constitutive model for C25 concrete are listed in Table 1 (Zhang et al. 2014; Xu and Wen 2016; Xu et al. 2019; Gao and Zhai 2022).

### 3 Results and Discussions

The parameters of a basic example are as follows: the diameter of the rock was 2 m, the impact velocity was 10 m/s, the impact height was 5 m, and the

solution time was 0.3 s. The test results of Nakajima et al. (2021) show that the time history curve of rock and concrete under impact is a spike pulse curve. The time history curve of impact force obtained by numerical simulation in this paper is shown in Fig. 4, and it is consistent with the pulse curve measured by Nakajima et al. It can be seen that under the same impact energy and impact point, the impact force of the concave dam was the smallest, with 29.13 MN, while the convex dam was the largest, with 39.72 MN.

**Table 1** Parameters of Holmquist-Johnson-Cook (HJC) model for C25 concrete

Symbol	Parameter	Value
$\rho_0$ (kg/m <sup>3</sup> )	Mass density	2400
$G$ (GPa)	Shear modulus	11.67
$A$	Normalized cohesive strength	0.79
$B$	Normalized pressure hardening	1.6
$C$	Strain rate coefficient	0.007
$N$	Pressure hardening exponent	0.61
$f'_c$ (GPa)	Quasi-static uniaxial compressive strength	0.0167
$T$ (GPa)	Maximum tensile hydrostatic pressure	0.00178
$\dot{\epsilon}_0$	Quasi-static threshold strain rate	1
$E_{fmin}$	Plastic strain before fracture	0.055
$S_{fmax}$	Normalized maximum strength	7
$P_c$ (GPa)	Crushing pressure	0.00557
$\mu_c$	Crushing volumetric strain	0.000359
$P_l$ (GPa)	Locking pressure	0.2785
$\mu_l$	Locking volumetric strain	0.1
$D_1$	Damage constant 1	0.04
$D_2$	Damage constant 2	1
$K_1$ (GPa)	Pressure constant 1	85
$K_2$ (GPa)	Pressure constant 2	-171
$K_3$ (GPa)	Pressure constant 3	208
$F_s$	Failure type	0.1

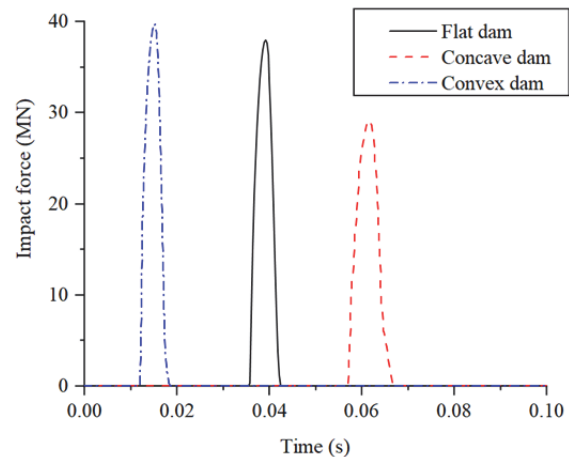


**Fig. 4** Time-history curve of impact force. The diameter of the boulder was 2 m, the impact speed was 10 m/s, and the impact point height was 5 m.

The impact force of the flat dam was between the two, at 37.94 MN. It can be observed from the above comparison that when the impact energy is 523 kJ, the concave impact force of the arch dam accounts for 73% of the convex dam and 77% of the flat dam.

Fig. 5 shows the energy time history curve of the flat dam. It can be seen from the figure that the overall energy of the structure was conserved, and the hourglass energy was 3% of the internal energy, which was less than 5% of the internal energy, so the numerical simulation results were reliable.

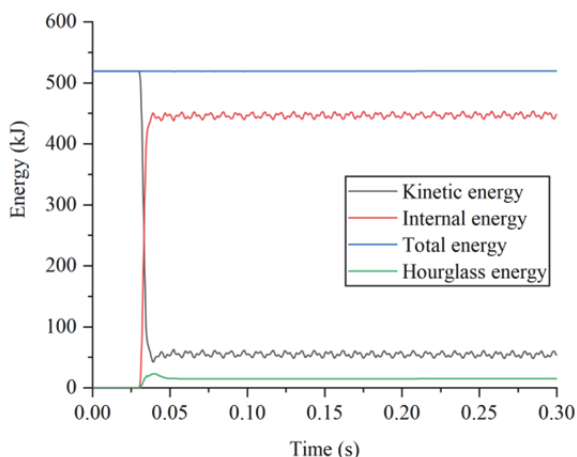


Fig. 5 Energy time history curve of the flat dam.

When the dam is impacted by a boulder, local damage occurred, and the damage location was mainly at the impact point. We selected Fcomp (fringe component) and Misc (history var#1) in ANSYS/LS-DYNA special post-processing software LS-PrePost to output the damage contour of the concrete HJC model (Fig. 6). It can be seen that the pits were obvious at the impact point. The impact range of a boulder was small and will not affect the overall safety of the retaining dam. This phenomenon is consistent with the research of Majeed et al. (2021). By counting the volume of deleted elements, three types of dam damage can be obtained. The volume of deleted elements of the flat dam, convex dam, and concave dam were 16370 mm<sup>3</sup>, 19120 mm<sup>3</sup>, and 12850 mm<sup>3</sup>, respectively. From the analysis results, it can be seen that the convex dam has the largest and the most serious damage, which is proportional to the impact force.

According to the momentum theorem, which is  $F\Delta t = m\Delta v$ , under the same conditions of impact mass and velocity, the impact force decreases with an increase in impact contact time. From the analysis results, it is known that the contact time of the concave, flat, and convex dam was 9.29 ms, 6.61 ms, and 6.59 ms, respectively.

Therefore, it can be known that the impact force of the concave dam is the least due to the contact time of the concave dam being the longest.

### 3.1 Analysis of impact force

First, the impact force of the flat dam is analyzed as follows. Many factors are affecting the impact force, among them, the impact velocity has a very significant

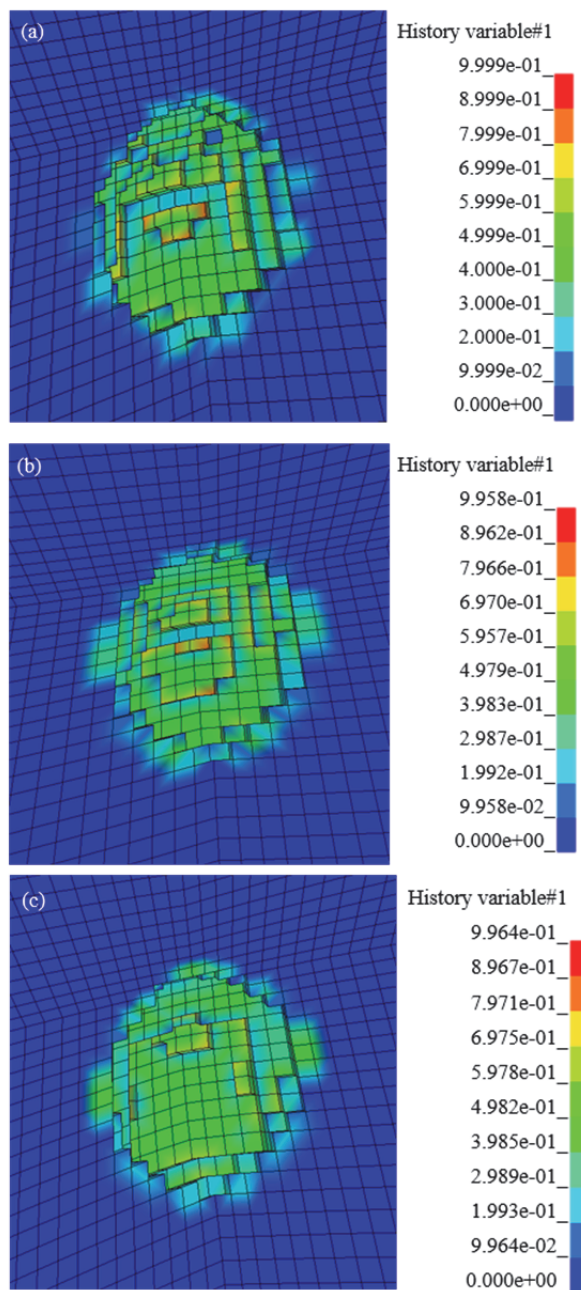


Fig. 6 Damage contour of dam models at impact point: (a) flat dam; (b) convex dam; (c) concave dam.



influence on the peak impact force under the condition that other factors are relatively fixed (Zhang et al. 2018; Franke et al. 2022). We studied the relationship between the peak impact force and the velocity of rock with a density of 2500 kg/m<sup>3</sup> at diameters of 1.0 m, 1.5 m, 2.0 m, 2.5 m, and 3.0 m while the impact point height remains 5.0 m.

The results show that the peak impact force increased with an increase in velocity under five different impact masses, and the relationship between them was linear growth. So the linear relation  $y = A + Bx$  was established to fit them, and the fitting results are presented in Table 2.

**Table 2** Fitting results between peak impact force and velocity under different masses

<i>D</i> (m)	<i>M</i> (kg)	<i>F</i>	A	B	SD	<i>R</i>
1.0	1038	F1	2.6955	1.0639	0.1666	0.9990
1.5	4416	F2	5.1118	2.0430	0.2159	0.9995
2.0	10467	F3	7.1106	3.0527	0.3489	0.9995
2.5	20443	F4	10.471	4.0255	0.7435	0.9986
3.0	35325	F5	14.4803	5.1743	1.4447	0.9968

**Notes:** *D* is the diameter of boulders; *M* is the mass of boulders; *F* is the impact force of boulders; SD stands for standard deviation; *R* stands for a correlation coefficient.

When the velocity is constant, both the impact kinetic energy and the impact force increase as the impact mass increases. Fig. 7 shows the relationship between the peak impact force with different velocities and the impact masses. It can be seen that under the condition of constant velocity, the peak impact force increased with an increase in the impact mass. But there was no linear relationship between the two. Additionally, under the condition that the impact mass was constant, as the velocity of the impact increased, the peak impact force also increased.

It should be noticed that the peak impact force has a non-linear relationship with the impact mass, and its growth trend was more in line with a rule of a power function. So power function was used to fit it. The power function form was  $y = ax^b$ . Subsequently, a set of coefficients *a* and *b* were obtained by fitting the impact force curves from 5 m/s to 15 m/s. It was found that the maximum variation of coefficients *b* was only 3%. Therefore, the average value of coefficient *b* was chosen as a fixed value, which is  $\bar{b}$ . Then the impact force and impact mass relationship curves at different velocities were fitted again, and different values of *a'* were obtained. The related

process is listed in Table 3. It can be seen from the table that the peak impact force and the impact mass had a good correlation at various velocities with a correlation coefficient (*R*) equal to 0.99, and the fitting was feasible.

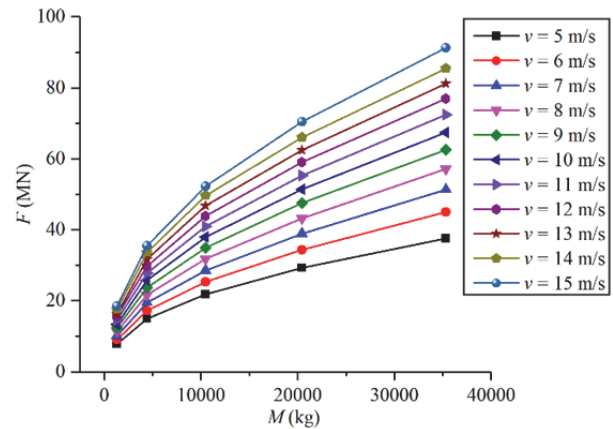


**Fig. 7** Relation between peak impact force (*F*) and impact mass (*M*) under different velocities (*v*).

**Table 3** Fitting results between peak impact force and mass under different velocities

<i>v</i> (m/s)	First fitting			Second fitting		
	<i>a</i>	<i>b</i>	<i>R</i>	<i>a'</i>	$\bar{b}$	<i>R</i>
5	0.3193	0.4553	0.9995	0.2760	0.47	0.9992
6	0.3127	0.4744	0.9997	0.3266	0.47	0.9996
7	0.3334	0.4806	0.9996	0.3706	0.47	0.9994
8	0.3762	0.4793	0.9997	0.4125	0.47	0.9996
9	0.4151	0.4786	0.9997	0.4523	0.47	0.9996
10	0.4642	0.4753	0.9997	0.4892	0.47	0.9996
11	0.5166	0.4718	0.9997	0.5259	0.47	0.9997
12	0.5773	0.4671	0.9997	0.5607	0.47	0.9997
13	0.6252	0.4647	0.9994	0.5934	0.47	0.9994
14	0.6951	0.4595	0.9995	0.6264	0.47	0.9993
15	0.6936	0.4661	0.9997	0.6670	0.47	0.9996

**Notes:** *v* is the velocity of boulders; *R* stands for the correlation coefficient.

Through the above fitting process, the relationship between peak impact force and impact mass was obtained as Eq. (2):

$$F = a \cdot M^{0.47} \tag{2}$$

where *a* is a correlation coefficient between the peak impact force and the impact mass.

Based on the above fitting process, we assumed that coefficient *a* has a certain relationship with velocity; the curve between coefficient *a* and velocity was plotted in Fig. 8. It was found that coefficient *a* was linear with velocity, and the relationship between coefficient *a* and velocity was obtained. The relationship between peak impact force, mass, and

velocity was expressed by Eq. (3):

$$F = (0.1007 + 0.0381v)M^{0.47} \quad (3)$$

where:  $F$ —Peak impact force (MN);

$v$ —Impact velocity (m/s);

$M$ —Impact mass (kg).

Using the same method, the peak impact force of the convex ( $F_{cv}$ ) and concave ( $F_{cc}$ ) dam was obtained as Eq. (4) and Eq. (5):

$$F_{cv} = (0.1349 + 0.0701v)M^{0.41} \quad (4)$$

$$F_{cc} = (0.0157 + 0.0318v)M^{0.50} \quad (5)$$

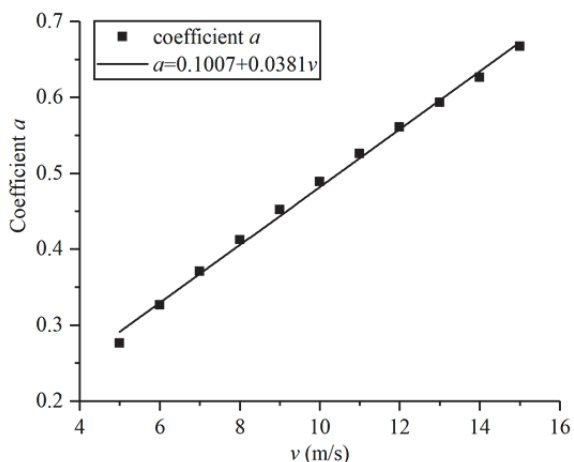


Fig. 8 Relationship between coefficient  $a$  and velocity ( $v$ ).

### 3.2 Effect of the height of impact points on the peak impact force

Previous studies have mostly considered the dynamic response of the dam when the height of the impact point of a dam was fixed, but the height of the impact point of a dam in actual disasters is random. This section considers the influence of different impact point heights on the impact force of a dam under the following three conditions: (1) the influence of different dam types on the impact force of a dam under the same impact energy. The diameter of the impactor was 2 m, and the impact velocity was 10 m/s (Fig. 9(a)); (2) the influence of different impactor velocities on the impact force of a dam under the same dam types. The diameter of the impactor was 2 m, the dam type was a flat dam (Fig. 9(b)); (3) the influence of different impactor diameters on the impact force of a dam under the same dam types. The impact velocity was 10 m/s, and the dam type was a flat dam (Fig. 9(c)). It should be noticed that other

conditions were the same as that before. The relationship between the impact point height and the peak impact force is shown in Fig. 9.

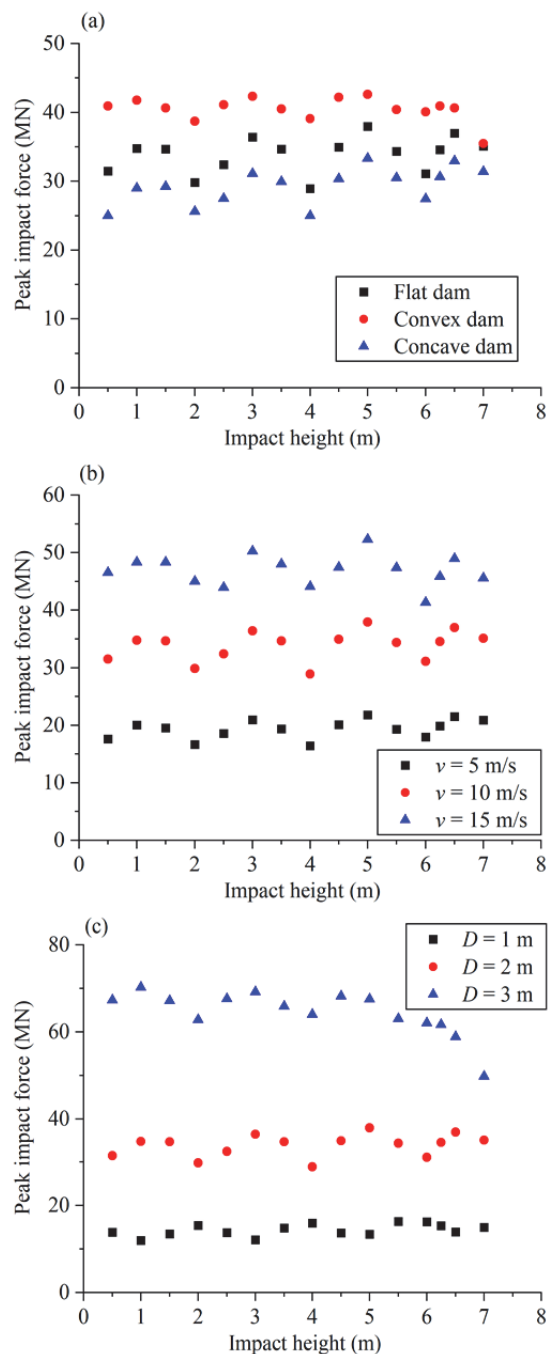


Fig. 9 Influence of impact point height on peak impact force: (a) different dam types; (b) different velocities of impactors; (c) different diameters of impactors.

It can be seen that when the impact energy is constant, the peak impact force on the dam fluctuates with the height of the impact point, and it reaches the maximum at the height of 5 m in different dam forms.

In other words, when the height of the impact point is 2/3 of the dam height, the peak value of impact force is the maximum. Moreover, for the flat dam, the peak impact force fluctuates with the height of the impact point as the velocity is different. The peak impact force is the largest when the height of the impact point is 2/3 of the dam height as well. Additionally, with the different diameters of the impactor, the peak impact force still fluctuates with the height of the impact point, but the position of the maximum peak impact force does not follow the previous rule. The above results show that with the change of the diameter of the impactor, there are differences in the fluctuation phenomenon of peak impact force, and there is no obvious rule to follow the impact position of the maximum peak impact force.

Reasons for the above phenomenon may be considered as follows: the characteristics of the wave transmitted by a solid with a certain mass on the surface of the object are certain. When the solid is impacted at different positions, different waves will be transmitted, and the superposition of waves at different positions will increase or decrease the wavelet intensity, resulting in the fluctuation trend of the peak impact force.

As reported above, when the impact energy is the same, the peak impact force of different dam types fluctuates with the height of the impact point, and the maximum peak impact force is obtained when the impact point height is a specific value. At the same time, for the same flat dam, the maximum peak impact force can also be obtained at the same impact point height when the impactor velocity is different. This effect can be considered an inherent characteristic of dams. However, this characteristic changes when the diameter of impactors varies.

In summary, the peak impact force changes little with the variation of impact height, indicating that the influence of the impact height factor is not very large and the rule is not obvious. Since the impact point height has little influence on the peak value of the impact force, and the rule is difficult to find, the influence of the impact point height on the peak impact force is not considered when fitting it.

### 3.3 Comparative analysis

The most common contact model considers the impact of elasticity and references Hertz's theory of contact between two elastic spheres to assess the

impact force. In this case, the peak impact force depends primarily on impact velocity. Meanwhile, elastic parameters are affected by body materials and the mass of a boulder (Yu et al. 2018; Nakajima et al. 2021). Take a flat dam as an example, and make the following comparison.

The impact force  $F$  (N) based on Hertz's formula is shown in Eq. (6):

$$F = n\alpha^{3/2} \tag{6}$$

where  $n$  and  $\alpha$  can be derived from Eq. (7) and Eq. (8).

$$n = \frac{4R_2^{0.5}}{3\pi(k_1 + k_2)} \tag{7}$$

$$\alpha = \left( \frac{5m_2v_2^2}{4n} \right)^{2/5} \tag{8}$$

$R_2$  (m) in Eq.(7) is the radius of a boulder,  $m_2$  (kg) in Eq.(8) is the mass of boulders,  $v_2$  (m/s) is the velocity of boulders normal to the barrier wall,  $k_1$  and  $k_2$  are coefficients related to Young's modulus (N/m<sup>2</sup>), Poisson ratios of boulders and barrier wall, as shown in Eq. (9) and Eq. (10):

$$k_1 = \frac{1-\nu_1^2}{\pi E_1} \tag{9}$$

$$k_2 = \frac{1-\nu_2^2}{\pi E_2} \tag{10}$$

In addition, for the design of rockfall protection in Japan (handbook for rockfall measures), the impact force of rockfall is estimated as Eq. (11) (CJRA 2000):

$$P=2.108 \cdot (mg)^{2/3} \lambda^{2/5} H^{3/5} \tag{11}$$

where  $P$  is impact force (kN),  $m$  is the mass of a rockfall (t),  $g$  is a gravity acceleration with 9.8 m/s<sup>2</sup>,  $\lambda$  is the Lamé constant of a sand cushion (kN/m<sup>2</sup>), and  $H$  is the height of a drop (m). The value of the Lamé constant  $\lambda$  is usually 10<sup>6</sup>.

Furthermore, combined with the experimental method, Labiouse et al. (1996) proposed a semi-theoretical and semi-empirical algorithm of rolling stone impact force as Eq. (12):

$$P = 1.765M_E^{2/5} R^{1/5} (QH)^{3/5} \tag{12}$$

where  $P$  is maximum impulsive force (kN),  $M_E$  is the modulus of subgrade reaction (kN/m<sup>2</sup>),  $R$  is the radius of the falling block part (m),  $Q$  is the weight of

the falling block (kN) and  $H$  is the falling height (m).

The impact force values of the above three formulae are compared by numerical calculation as follows. In the comparison, the impact velocity was selected from 5 m/s to 15 m/s, and the diameter of the impactor was 1 m, 2 m, and 3 m. The results of the comparison Eq. (6), Eq. (11), Eq. (12) with the empirical formula Eq. (3) are illustrated in Fig. 10. It can be observed that when the impact diameter is 1 m and the impact mass is 1038 kg, the empirical formula in this paper is in good agreement with the existing results. It is worth noting that when the impact mass is large, the impact force calculated by references (Hertz 1881; Labiouse et al. 1996; CJRA 2000) is larger than the value in this paper. This result is consistent with Zhang et al.'s findings (2018). In addition, this trend increases with an increase in impact mass and velocity.

Because Eq. (6), Eq. (11), and Eq. (12) are derived from the theory of elastic collision. Thus it ignored the effects of friction and damage, which can dissipate energy. Therefore, when a boulder impacts a concrete dam, this situation does not fully conform to the elastic impact theory and will cause energy loss, e.g., cracks and damage on the impact surface. In this paper, the friction between the contact surfaces and the damage to the dam is considered when selecting the material model. The impact force is smaller than the existing theory when the impact mass and velocity are larger, which trend is also consistent with several studies (Ng Charles et al. 2021; Luo et al. 2022).

Although there are no consistent field tests, we compared several similar experimental and field tests as shown in Fig. 11. It can be seen from the figure that the empirical formula is always greater than the measured value. The main reasons are analyzed as follows:

The experiments of Labiouse et al. (1996) studied the dynamic response of reinforced concrete rock sheds impacted by rock blocks, and mainly investigated the damping capacity of different material cushions. Rockfall weights were 100, 500, and 1000 kg. The thicknesses of the soil cushion were 0.35, 0.50, and 1.00 m, and the soil cushion material included concrete gravel, alluvial cones, and scrap rocks with a density of 1650, 1890, and 1790 kg/m<sup>3</sup>. The size of the concrete slab was 3.4 m×3.4 m, the thickness was 0.2 m, and the concrete strength grade was B35/25. The impact force was converted from the value measured by the accelerometer on the falling

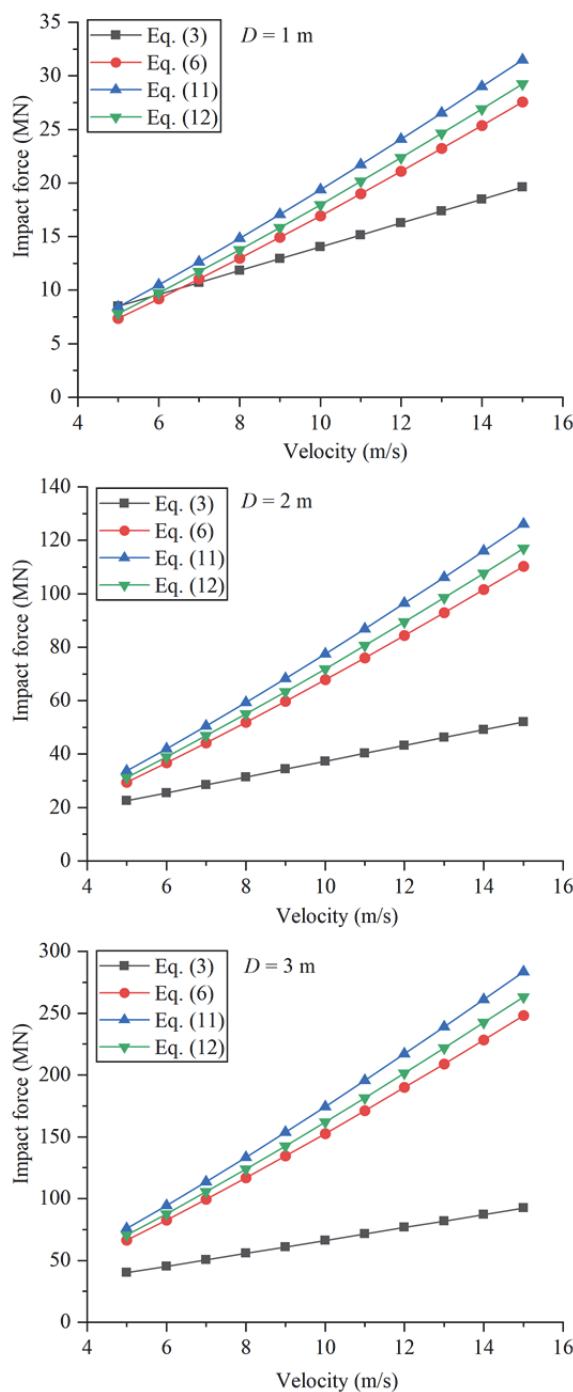


**Fig. 10** Comparison between empirical formula and theoretical formula of peak impact force under different impactor diameters (the impact point height was 5 m).

block. It can be seen from Fig. 11(a) that the main reason why the calculated value is greater than the measured value is that the presence of the 0.5 m gravel cushion significantly reduces the impact force during the test. In addition, the lower density of the rockfall also reduces the impact force.



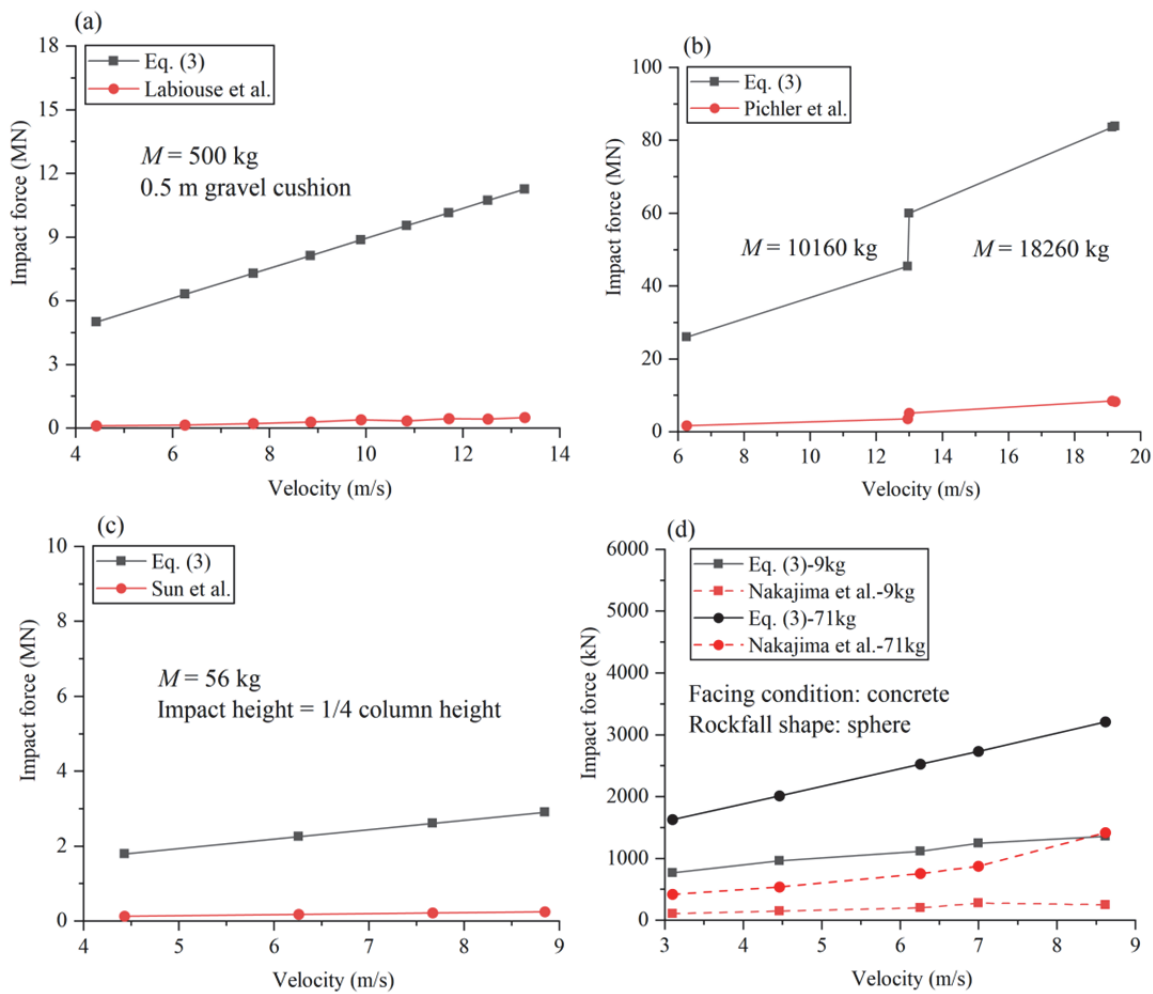


**Fig. 11** Impact force vs velocity between empirical formula and experimental tests: (a) Labiouse et al. (1996); (b) Pichler et al. (2005); (c) Sun et al. (2021); (d) Nakajima et al. (2021).

The experiments of Pichler et al. (2005) studied the impact of rocks onto gravel, and the relationships between penetration depth, impact duration and impact force and rock boulder mass, drop height and gravel resistance to indentation were given. The boulder in the test was granite with a density of 2700 kg/m<sup>3</sup>, the rock-boulder mass was limited to 20000 kg, and the drop height was restricted to 20 m. The mass density of gravel was equal to 1800 kg/m<sup>3</sup>. The acceleration of the rock in the vertical direction was measured by equipping each boulder with an accelerometer. It can be seen from Fig. 11(b) that the main reason why the impact force of the empirical formula is greater than the test value is that the impacted object is gravel, whose density is much lower than that of concrete, and it acts as a buffer layer, so the impact force is significantly reduced.

The experiments of Sun et al. (2021) studied the

damage after rockfall impacted the bridge pier. A 56 kg pendulum device was designed to impact a 1/4 scale concrete model column to simulate a rockfall impacting a bridge pier. The impact point positions were 1/4, 3/8, and 1/2 of the column height. The bridge pier model with a diameter of 300 mm and a height of 2500 mm was made of C30 concrete. The impact material was a solid steel ball. During the test, the impact force was measured by fixing the impact sensor on the spherical impact head. It can be seen from the results in Fig. 11(c) that the impact force calculated by the empirical formula is greater than the measured value. The reason for this difference is that there is an essential difference in the form of the impacted object. The stiffness of the reinforced concrete column is significantly smaller than that of the concrete dam, and the impact force is reduced due to the reduction of the stiffness.

Nakajima et al. (2021) conducted a series of experiments to understand the effect of weight, size, shape, stiffness, material, and motion type of the impact object on the impact force. During the test, the drop weight was free-falling onto the reaction unit, which was supported by five H-shaped steel piles with a length of 5 m, on which three-component load cells were installed. In addition, using concrete or wood plate as the facing material of the load cell, the effect of the facing stiffness of the protective wall on the impact force was studied. Rockfall materials included natural real rocks, rock models (sphere, block, and plate), and deformable soil. It can be seen from Fig. 11(d) that the impact force value of the empirical formula is greater than the measured value. The reason for this difference is also the reduction of the impact surface stiffness because the stiffness of the thin concrete surface is lower than that of the concrete dam.

In summary, the proposed empirical formulae for the peak impact force of the dam are suitable for concrete flat dams, convex dams, and concave dams with a height of 7.5 m, length of 14 m, and an average thickness of 2.3 m (arch dam radius  $R = 8.6$  m), respectively. The impact mass range is 1038~35325 kg, the impact velocity range is 5~15 m/s, and the impact direction is parallel to the ground. In our further research, we will consider the dynamic response of double curvature arch dam and variable curvature arch dam as well as the impact resistance of arch dam under different curvatures. This paper only considered the dynamic response of flat dams and single curvature arch dams under different impact directions.

## 4 Conclusions

In deep mountain canyons, concrete dams are often damaged by boulders. It is of great significance to consider the dynamic impact of different dam types under impact loads. In this paper, three finite element models of dams considering the HJC damage material

## References

China Geological Disaster Prevention Engineering Association (2018) Specification of Design for Debris Flow Prevention (T/CAGHP 021). p 63 (In Chinese)  
Bozdağ A (2022) Rockfall hazard assessment in a natural and

model are established. The time history of impact force and dynamic response of dam under different parameters are obtained by LS-DYNA explicit analysis. The following conclusions are drawn:

(1) By analyzing the peak impact force at different impact points, it was found that the influence of the height of the impact point on the impact force fluctuates with different impact heights, but the fluctuation amplitude is not large. When the height of the impact point is 2/3 of the dam height, the peak impact force of the dam reaches the maximum, and this impact position does not change with the variation of dam type (i.e., flat dam, concave dam, and convex dam) and impactor velocity (i.e., the impact velocity is 5, 10, and 15 m/s).

(2) Through a large number of data fitting of different parameters, the empirical formulae of the impact force under three different dam types are given, which can be used as a reference for similar dam designs. Meanwhile, by comparison with other classical calculation methods and experimental and field tests of impact force, it can be seen that the proposed empirical formula is reasonable and effective. With the increase in the mass and velocity of the impactor, the empirical formula value proposed in this paper is lower than the Hertz theoretical, the Japanese manual, and the model of Labiouse et al while larger than the experimental and field tests.

(3) When the concrete dam is impacted by a boulder, local damage occurs, and the damage location is mainly at the impact point. There are obvious differences in the impact force of the concave dam and the convex dam under the impact load compared with the ordinary flat dam. When the impact energy is 523 kJ, the concave impact force of the arch dam accounts for 73% of the convex impact force, and 77% of the flat dam impact force.

## Acknowledgments

This work was supported by the National Natural Science Foundation of China (Grant No. 51778273).

historical site: The case of ancient Kilistra settlement (Konya), Turkey. J Mt Sci 19(1): 151-166.  
<https://doi.org/10.1007/s11629-021-6961-6>  
Cappadonia C, Cafiso F, Ferraro R, et al. (2021) Rockfall hazards

- of Mount Pellegrino area (Sicily, Southern Italy). *J Maps* 17(3): 29-39.  
<https://doi.org/10.1080/17445647.2020.1824826>
- CJRA (2000) Handbook for rockfall measures. Compilation by Japan Road Association. (In Japanese)
- Dowling CA and Santi PM (2014) Debris flows and their toll on human life: a global analysis of debris-flow fatalities from 1950 to 2011. *Nat Hazard* 71(1): 203-227.  
<https://doi.org/10.1007/s11069-013-0907-4>
- Evans SG and Hungr O (1993) The assessment of rockfall hazard at the base of talus slopes. *Can Geotech J* 30(4): 620-636.  
<https://doi.org/10.1139/t93-054>
- Ferrari F, Giacomini A and Thoeni K (2016) Qualitative rockfall hazard assessment: a comprehensive review of current practices. *Rock Mech Rock Eng* 49(7): 2865-2922.  
<https://doi.org/10.1007/s00603-016-0918-z>
- Franke F, Schwab M, Burger U, et al. (2022) An analytical model to determine the impact force of drone strikes. *CEAS Aeronaut J* 13(1): 69-84.  
<https://doi.org/10.1007/s13272-021-00552-4>
- Gang L, Hu XW, Du YJ, et al. (2019) A collision fragmentation model for predicting the distal reach of brittle fragmentable rock initiated from a cliff. *Bull Eng Geol Environ* 78(1): 579-592.  
<https://doi.org/10.1007/s10064-018-1286-6>
- Gao FF and Tian W (2020) Dynamic response analysis of blocks-combined dam under impact load. *J Mt Sci* 17(11): 2827-2839.  
<https://doi.org/10.1007/s11629-019-5619-0>
- Gao G, Meguid Mohamed A, Chouinard Luc E, et al. (2020) Insights into the Transport and Fragmentation Characteristics of Earthquake-Induced Rock Avalanche: Numerical Study. *Int J Geomech* 20(9): 04020157.  
[https://doi.org/10.1061/\(ASCE\)GM.1943-5622.0001800](https://doi.org/10.1061/(ASCE)GM.1943-5622.0001800)
- Gao H and Zhai Y (2022) Numerical investigation of the concrete-rock combined body influence of inclined interface on dynamic characteristics and failure behaviors. *Arabian J Geosci* 15(5): 435.  
<https://doi.org/10.1007/s12517-022-09749-1>
- Gao Y, Yin YP, Li B, et al. (2018) Characteristics and numerical runout modeling analysis of the Jiweishan Landslide, Chongqing, China. *Environ Eng Geosci* 24(4): 413-423.  
<https://doi.org/10.2113/EEG-1916>
- Hertz H (1881) On the contact of elastic solids. *J Reine Angew Math* 92: 156-171.  
<https://doi.org/10.1103/PhysRevA.31.1957.3>
- Holmquist TJ, Johnson GR and Cook WH (1993) A computational constitutive model for concrete subjected to large strains, high strain rate, and high pressures. 14th international symposium on ballistics, Quebec, Canada. pp 591-600.
- Huang Y and Zhang B (2020) Challenges and perspectives in designing engineering structures against debris-flow disaster. *Eur J Environ Civ Eng* 26(10): 4476-4497.  
<https://doi.org/10.1080/19648189.2020.1854126>
- Im S, Yi S and Eu S (2017) Implementation of a flexible wire net dam for controlling debris flow in a small mountain torrent. In: Mikos M, Arbanas Z, Yin Y, et al. (eds) *Advancing Culture of Living with Landslides, Vol 3: Advances in Landslide Technology*. Cham: Springer International Publishing Ag. pp 503-511.  
[https://doi.org/10.1007/978-3-319-53487-9\\_59](https://doi.org/10.1007/978-3-319-53487-9_59)
- Jin YT, Yu ZX, Luo LR, et al. (2021) A membrane equivalent method to reproduce the macroscopic mechanical responses of steel wire-ring nets under rockfall impact. *Thin-Walled Struct* 167: 108227.  
<https://doi.org/10.1016/j.tws.2021.108227>
- Johnson KL (1985) *Contact mechanics*. New York: Cambridge University Press. p 452.
- Kang C, Ren DX, Gao XF, et al. (2021) Study of kinematic characteristics of a rock avalanche and subsequent erosion process due to a debris flow in Wenjia gully, Sichuan, China. *Nat Hazard* 106(1): 937-964.  
<https://doi.org/10.1007/s11069-021-04501-6>
- Kim Y, Nakagawa H, Kawaike K, et al. (2017) Study on hydraulic characteristics of sabo dam with a flap structure for debris flow. *Int J Sediment Res* 32(3): 452-464.  
<https://doi.org/10.1016/j.ijsrc.2017.05.001>
- Labiousse V, Descoedres F and Montani S (1996) Experimental study of rock sheds impacted by rock blocks. *Struct Eng Int* 6: 171-176.  
<https://doi.org/10.2749/101686696780495536>
- Liu C, Phuong N and Zhao SC (2021) Dynamic response of RC sheds against the impact of rock block with different shapes and angles. *Can J Civ Eng* 49(6): 870-884.  
<https://doi.org/10.1139/cjce-2021-0146>
- Long XH, Turgun A, Yue R, et al. (2018) Influence factors analysis of rc beams under falling weight impact based on HJC Model. *Shock Vib* 2018: 4731863.  
<https://doi.org/10.1155/2018/4731863>
- Luo G, Zhao YJ, Shen WG, et al. (2022) An analytical method for the impact force of a cubic rock boulder colliding onto a rigid barrier. *Nat Hazard* 112(1): 603-618.  
<https://doi.org/10.1007/s11069-021-05196-5>
- Majeed ZZA, Lam NTK and Gad EF (2021) Predictions of localised damage to concrete caused by a low-velocity impact. *Int J Impact Eng* 149: 103799.  
<https://doi.org/10.1016/j.ijimpeng.2020.103799>
- Malvar LJ, Crawford JE, Wesevich JW, et al. (1997) A plasticity concrete material model for DYNA3D. *Int J Impact Eng* 19(9-10): 847-873.  
[https://doi.org/10.1016/S0734-743X\(97\)00023-7](https://doi.org/10.1016/S0734-743X(97)00023-7)
- Murray YD (2007) User's manual for LS-DYNA concrete material model 159. Report No.FHWA-HRT-05-062, Washington, D.C., USA: Federal Highway Administration.
- Nakajima S, Abe K, Shinoda M, et al. (2021) Experimental study on impact force due to collision of rockfall and sliding soil mass caused by seismic slope failure. *Landslides* 18(1): 195-216.  
<https://doi.org/10.1007/s10346-020-01461-z>
- Ng Charles WW, Liu H, Choi Clarence E, et al. (2021) Impact dynamics of boulder-enriched debris flow on a rigid barrier. *J Geotech Geoenviron Eng* 147(3): 04021004.  
[https://doi.org/10.1061/\(ASCE\)GT.1943-5606.0002485](https://doi.org/10.1061/(ASCE)GT.1943-5606.0002485)
- Othman A, Shaaban F, Abotalib AZ, et al. (2021) Hazard assessment of rockfalls in mountainous urban areas, Western Saudi Arabia. *Arabian J Sci Eng* 46(6): 5717-5731.  
<https://doi.org/10.1007/s13369-020-05098-x>
- Ouyang CJ, Zhou KQ, Xu Q, et al. (2017) Dynamic analysis and numerical modeling of the 2015 catastrophic landslide of the construction waste landfill at Guangming, Shenzhen, China. *Landslides* 14(2): 705-718.  
<https://doi.org/10.1007/s10346-016-0764-9>
- Pichler B, Hellmich C and Mang HA (2005) Impact of rocks onto gravel design and evaluation of experiments. *Int J Impact Eng* 31(5): 559-578.  
<https://doi.org/10.1016/j.ijimpeng.2004.01.007>
- Pla B, Kr B, Zheng L, et al. (2020) Experimental and numerical study on the performance of novel RC frame structure encased with shaped steel under debris flow impact. *Eng Struct* 212: 1-16.  
<https://doi.org/10.1016/j.engstruct.2020.110472>
- Riedel W, Thoma K, Hiermaier S, et al. (1999) Penetration of reinforced concrete by BETA-B-500 numerical analysis using a new macroscopic concrete model for hydrocodes. *Proceedings of the 9th International Symposium on the Effects of Munitions with Structures*. Berlin-Strausberg Germany. pp 315-322.
- Sekhar J (2018) Tunable coefficient of friction with surface texturing in materials engineering and biological systems. *Curr Opin Chem Eng* 19: 94-106.  
<https://doi.org/10.1016/j.coche.2017.12.002>
- Shieh CL, Ting CH and Pan HW (2008) Impulsive force of

- debris flow on a curved dam. *Int J Sediment Res* 23(2): 149-158.  
[https://doi.org/10.1016/S1001-6279\(08\)60014-1](https://doi.org/10.1016/S1001-6279(08)60014-1)
- Su ZY, Zhang K and Liu CD (2022) Dynamic risk assessment of slope stability of homogeneous earth-rock dam under action of multiple hazards. *Simul* 98(8): 699-710.  
<https://doi.org/10.1177/00375497211073772>
- Sun X, Bi Y, Zhou R, et al. (2021) Experimental study on the damage of bridge pier under the impact of rockfall. *Adv Civ Eng* 2021: 6610652.  
<https://doi.org/10.1155/2021/6610652>
- Taylor LM, Chen EP, Kuszmaul JS (1986) Microcrack-induced damage accumulation in brittle rock under dynamic loading. *Comput Methods Appl Mech Eng* 55(3): 301-320.  
[https://doi.org/10.1016/0045-7825\(86\)90057-5](https://doi.org/10.1016/0045-7825(86)90057-5)
- Ulamış K, Kılıç R (2020) Combined instability assessment and rockfall hazard in volcanic rocks (Keçiören, Ankara). *Arabian J Geosci* 13(10): 349.  
<https://doi.org/10.1007/s12517-020-05338-2>
- Wan WZ, Yang J, Xu GJ, et al. (2021) Determination and evaluation of Holmquist-Johnson-Cook constitutive model parameters for ultra-high-performance concrete with steel fibers. *Int J Impact Eng* 156(2021): 103966.  
<https://doi.org/10.1016/j.ijimpeng.2021.103966>
- Wang H, Lv Z, Zhang J, et al. (2020a) Internal force analysis of buried-boring piles in the Yuanzishan Landslide. *Appl Sci* 10(16): 5416.  
<https://doi.org/10.3390/app10165416>
- Wang H, Wang P, Qin H, et al. (2020b) Method to control the deformation of anti-slide piles in Zhenzilin Landslide. *Appl Sci* 10(8): 2831.  
<https://doi.org/10.3390/app10082831>
- Wei RQ, Zeng QL, Davies T, et al. (2018) Geohazard cascade and mechanism of large debris flows in Tianmo gully, SE Tibetan Plateau and implications to hazard monitoring. *Eng Geol* 233: 172-182.  
<https://doi.org/10.1016/j.enggeo.2017.12.013>
- Xu H, Wen HM (2016) A computational constitutive model for concrete subjected to dynamic loadings. *Int J Impact Eng* 91: 116-125.  
<https://doi.org/10.1016/j.ijimpeng.2016.01.003>
- Xu LY, Xu H, Wen HM (2019) On the penetration and perforation of concrete targets struck transversely by ogival-nosed projectiles - a numerical study. *Int J Impact Eng* 125: 39-55.  
<https://doi.org/10.1016/j.ijimpeng.2018.11.001>
- Yan CL, Tu J, Li DY, et al. (2021) The failure mechanism of concrete gravity dams considering different nonlinear models under strong earthquakes. *Shock Vib* 2021: 5558284.  
<https://doi.org/10.1155/2021/5558284>
- Yang JCS, Chun DS (1969) Application of the Hertz contact law to problems of impact in plates. Report No. NOLTR 69-152, Maryland: Naval Ordnance Lab, White Oak, MD.
- Yu B, Yi W, Zhao HB (2018) Experimental study on the maximum impact force by rock fall. *Landslides* 15(2): 233-242.  
<https://doi.org/10.1007/s10346-017-0876-x>
- Yu Z (2016) The mechanism of deformation and failure of debris flow dam under the shock load. Xi'an University of Science and Technology, Xi'an. (In Chinese)
- Zhang H, Xie A and Gao YW (2014) Numerical simulation of SHPB test for concrete under confining pressure. *Appl Mechs Mater* 580-583: 3144-3148.  
<https://doi.org/10.4028/www.scientific.net/AMM.580-583.3144>
- Zhang SL, Yang XG and Zhou JW (2018) A theoretical model for the estimation of maximum impact force from a rockfall based on contact theory. *J Mt Sci* 15(2): 430-443.  
<https://doi.org/10.1007/s11629-017-4606-6>